J. Chem. Sci. Vol. 128, No. 11, November 2016, pp. 1795–1804.
DOI 10.1007/s12039-016-1180-3

Catalytic decomposition of N_2O over CeO_2 supported Co_3O_4 catalysts

S K MAHAMMADUNNISA, T AKANKSHA, K KRUSHNAMURTY and CH SUBRAHMANYAM*

Energy and Environmental Research Lab, Department of Chemistry, Indian Institute of Technology, Hyderabad 502 205, Telangana, India
e-mail: csubbu@iith.ac.in

MS received 19 June 2016; revised 26 August 2016; accepted 12 September 2016

Abstract. This work was aimed to design efficient catalysts for N_2O decomposition at low temperatures. Cobalt oxide (Co_3O_4) was prepared by hydrothermal, precipitation and combustion methods and tested for N_2O decomposition. It was found that the catalysts prepared by solution combustion synthesis were most active for this reaction. Subsequently, a series of ceria (CeO_2) supported Co_3O_4 catalysts (xCeCo) were prepared by solution combustion method and used them for N_2O decomposition. All the catalysts were characterized by analytical methods like XRD, TEM, BET, XPS, UV-Vis, Raman and H_2-TPR. It was found that 10 and 20 wt..% loading of CeO_2 on Co_3O_4 promoted the activity of Co_3O_4 towards N_2O decomposition, whereas, higher loading of CeO_2 reduced the activity. Typical results indicated that addition of CeO_2 increases the surface area of Co_3O_4, and improves the reduction of Co^{3+} to Co^{2+} by facilitating the desorption of adsorbed oxygen species, which is the rate-determining step for the N_2O decomposition over Co_3O_4 spinel catalysts. Optimal CeO_2 loading can increase both dispersion and surface area of Co_3O_4 catalysts and weaken the Co–O bond strength to promote N_2O decomposition.

Keywords. Low temperature N_2O decomposition; cobalt oxide; ceria; solution combustion synthesis; citric acid.

1. Introduction

It has been reported that nitrous oxide (N_2O) is one of the ozone-depleting substances.[1] Also, with a global warming potential of nearly 300 times more than CO_2, N_2O is a potent greenhouse gas.[2] About 40% of global N_2O emissions are a result of human activities. Major sources are agriculture, transportation, combustion of fossil fuels and industries involved in preparation of adipic aid, nitric acid, *etc*. Apart from these, many natural processes like nitrogen cycle and breakdown of nitrogen by bacteria in soil and oceans are also responsible for N_2O emissions. Also, N_2O is released as a by-product during the abatement of other environmentally harmful species like three-way catalytic decomposition of NO_x, hydrocarbons, *etc*.[3] Hence the growing level of N_2O in atmosphere is a major concern. To curb this, many new ways of emission reduction are being investigated. Broadly there can be two possible ways; either controlling the amount of N_2O being released or decomposition of the released N_2O. Latter option turns out to be more realistic as a lot of time is needed to bring down the current emission levels. Catalytic decomposition of N_2O is an extensively studied area.[3] Starting from the usage of metals like Ir, Cu dispersed on suitable supports,[4,5] to metals supported with alkali dopants,[6,7] improvisations have been made by using pure, supported[8] and mixed metal oxides.[9–12] Among the various transition metal oxides, cobalt oxide (Co_3O_4) has shown promising activity for decomposition of N_2O. Co_3O_4 spinel has a cubic structure and is expected to have 1:2 ratio of Co^{+3}: Co^{+2} ions. However, the presence of non-stoichiometry results in an increased concentration of oxide ions, which in turn causes an increased ratio of Co^{+3} due to charge transfer to oxygen. Octahedral site is assumed to be the catalytically active site of pure cobalt oxide. However, an enhanced activity is seen if Co^{+3} is present instead of Co^{+2} in octahedral site.[13] The redox couple of Co^{+3}/Co^{+2} plays an important role in the usage of Co_3O_4 as catalyst in numerous other reactions like oxidation of Carbon monoxide (CO)[14] and ammonia (NH_3).[15] Pristine Co_3O_4 has numerous limitations for its use as catalyst for N_2O decomposition, especially at higher temperatures because of reduction of its active phase to CoO. Further, the catalyst particles tend to sinter and form clusters which results in reduced activity. Hence, a dopant is needed which apart from stabilizing the catalyst, may also provide additional and enhanced

*For correspondence

S K Mahammadunnisa and T Akanksha have equal contribution

catalytic activity. Among the various structural modifiers available, ceria (CeO_2) seems to be a good candidate because of its well-known 'oxygen storage capacity'. CeO_2 plays an important role in two most important industrial processes: three-way catalysis (TWC) and fluid catalytic cracking (FCC). Apart from this, CeO_2 has been used in the treatment of gaseous emissions like SOx, and liquid wastes. However, in all these processes it always acts as structural/electronic promoter and/or as co-catalyst.[16] Hence, effective stabilization of the dispersed state of transition metal oxides by preventing sintering, retention of their high surface area and its redox/oxidation properties along with high oxygen mobility further encourage the usage of CeO_2 in combination with CoOx.[17] Earlier Xue *et al*., had reported decomposition of N_2O over cerium oxide promoted cobalt oxide catalyst prepared by co-precipitation method.[18] However, it is well-known that catalyst activity can be modified by the preparatory methods.[19] With this background, we first prepared pure Co_3O_4 by using solution combustion, co-precipitation and hydrothermal synthesis and tested their activity for N_2O decomposition. Subsequently, the best one was chosen and was supported with varying amounts of CeO_2 so as to get a series of CeO_2 doped Co_3O_4 (xCeCo) catalysts and studied their activity for N_2O decomposition.

2. Experimental

2.1 *Catalyst preparation*

Co_3O_4 was prepared by three different preparation methods, namely solution combustion, co-precipitation and hydrothermal synthesis.

2.1.1 *Hydrothermal synthesis of Co_3O_4*: Cobalt nitrate, cetyltrimethyl ammonium bromide (CTAB) and urea were dissolved in calculated amount of water and stirred for 10 min. They were then transferred to a Teflon beaker and kept in an autoclave maintained at 160°C for 15 h. After the completion of reaction, contents were filtered and washed with water. They were then calcined at 500°C for 12 h so as to get the desired catalyst.

2.1.2 *Co-precipitation synthesis of Co_3O_4*: Cobalt nitrate was dissolved in optimum amount of water and was kept for stirring. To this, 2 M sodium hydroxide solution was added drop wise to maintain pH around 11. The precipitate so obtained was left undisturbed for ageing overnight. Later, it was filtered and washed with hot water. Solid so obtained was then calcined at 450°C for 12 h to get the desired catalyst.

2.1.3 *Solution combustion synthesis of Co_3O_4*: Cobalt nitrate hexahydrate, $Co(NO_3)_2$.$6H_2O$ (taken as cobalt precursor) and citric acid ($C_6H_8O_7$) (taken as fuel, purchased from Sigma) were dissolved in minimum amount of water and the solution was sonicated for 15 min. Fuel: oxidant ratio (Φ) was fixed at 1:1. The resultant solution was kept on hot plate so as to get froth. This was then placed inside a preheated furnace maintained at 450°C for 15 min. The spongy solid so obtained was crushed into a fine powder and stored for further characterization and reactions.

2.1.4 *Solution combustion synthesis of CeO_2 doped Co_3O_4 (xCeCo) catalysts*: A series of CeO_2 loaded Co_3O_4 catalysts was prepared by solution combustion method. Amount of CeO_2 was varied from 0 to 100% $\{100 * xCeO_2/((1-x)\ Co_3O_4 + xCeO_2)\}$ so as to get xCeCo catalysts where x denotes the mole fraction of CeO_2. Calculated amounts cobalt nitrate, ceric ammonium nitrate ($(NH_4)_2Ce(NO_3)_6{\cdot}6H_2O$) and citric acid were dissolved in minimum amount of water. Contents were sonicated for 15 min and later concentrated on a hot plate so as to get froth. Then they were taken inside a preheated furnace maintained at 450°C for 15 min. Solid so obtained was crushed to a fine powder so as to get desired xCeCo catalysts.

2.2 *Catalyst Characterization*

Synthesised catalysts were characterized by various methods such as XRD, Raman, BET and temperature programmed reduction (TPR). The as-synthesized samples were characterised by X-ray diffractometry using a computerized PAN analytical X'pert pro X-ray diffractometer using Cu Kα =1.541 Å radiation, 30 mA and 40 kV. The step scans were taken over a 2θ range of 0 to 90°. The N_2 adsorption-desorption isotherms were obtained by using NOVA 2200e equipment. Specific surface area was measured from these isotherms by applying the Brunauer-Emmett-Teller (BET) method. Raman spectra of the samples were obtained using Bruker senterra dispersive Raman microscope. Diffuse UV-Vis reflectance spectra of the Co_3O_4 catalysts prepared by different methods and xCeCo catalysts were collected using Shimadzu UV-Vis spectrophotometer (UV-3600) with a spectral grade $BaSO_4$ as reference. X-ray Photoelectron Spectroscopy (XPS) data of the combustion synthesized catalysts were recorded by

an Axis Ultra instrument under ultra-high vacuum conditions (10^{-8} Torr) and using a monochromatic Al Ka X-ray source (1486.6 eV). The Transmission Electron Microscopy (TEM) image was recorded using FEI model TECNAI G 220 S-Twin equipment. Temperature Programmed Reductions (TPR) experiments were carried out in a flow system (Quantachrome autosorb-IQ automated gas sorption Analyzer) equipped with a thermal conductivity detector (TPR-TCD). For TPR measurements, 50 mg of the sample was sandwiched between quartz wool plugs in a U-shaped quartz reactor and flushed with He for 30 min. The TPR profiles were obtained by heating the sample from room temperature to the desired temperature (600°C) in 10% H_2 in Ar, (gas flow rates 40 mL/min and heating rate of 10°C/min) and the gaseous products were sampled through a fine control leak valve to TCD after passing through a cold trap to remove H_2O. Quantitative analysis was done by integrating the reduction signal and comparison was made by pre-calibrated signals.

2.3 *Activity measurements*

In order to test for activity, 0.5 g of catalyst was placed in a quartz reactor which was then placed in a furnace maintained at 25°C. The inlet of the reactor was connected to N_2O (10% N_2O in Ar) gas maintaining a flow rate of 60 mL/min by using mass flow controllers (GFC-17, Aalborg-USA). Products were analysed by means of gas chromatography (Varian 450 GC) equipped with a thermal conductivity detector (TCD). The activation energy was estimated from the Arrhenius plot.[20] The conversion of N_2O was calculated as follows eq. (1),

$$\%\ of\ N_2O_{conv} = \frac{N_2O_{in} - N_2O_{out}}{N_2O_{in}} \times 100 \qquad (1)$$

3. Results and Discussion

3.1 *Characterization results*

3.1.1 *Powder X-Ray Diffraction (P-XRD) of Co_3O_4 catalysts*: Powder XRD patterns of Co_3O_4 prepared by combustion, co-precipitation and hydrothermal synthesis are shown in Figure 1. The patterns of Co_3O_4 show characteristic peaks of (220), (311), (222), (400), (511) and (520) planes, corresponding to Co_3O_4 spinel structure.

Figure 2 represents the XRD patters of xCeCo catalysts. The XRD patterns show prominent peaks at 2θ (deg) values of 19.1, 31.4, 36.8, 38.6, 44.9, 56.3, 59.3 and 65.4 which are indexed, respectively, as (111), (220), (311), (222), (400), (422), (511) and (440) planes of fcc structure of Co_3O_4 with space group of Fd_{3m} (227).[20] The diffraction lines corresponding to the ceria phase started appearing after 40% ceria content i.e., 40CeCo onwards. The intensity of Co_3O_4 signals increases with the cobalt content.

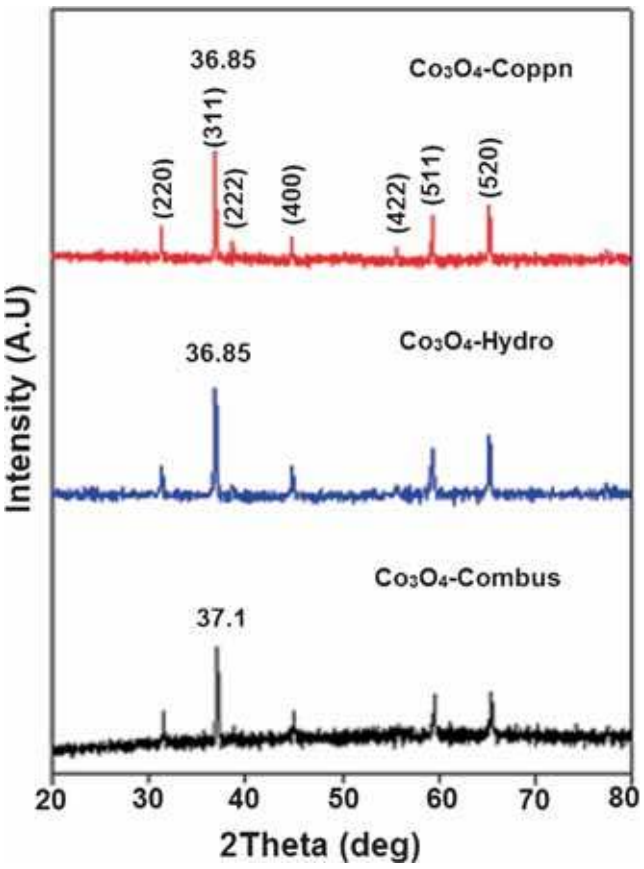

Figure 1. P-XRD pattern of Co_3O_4 catalysts prepared by different preparation methods.

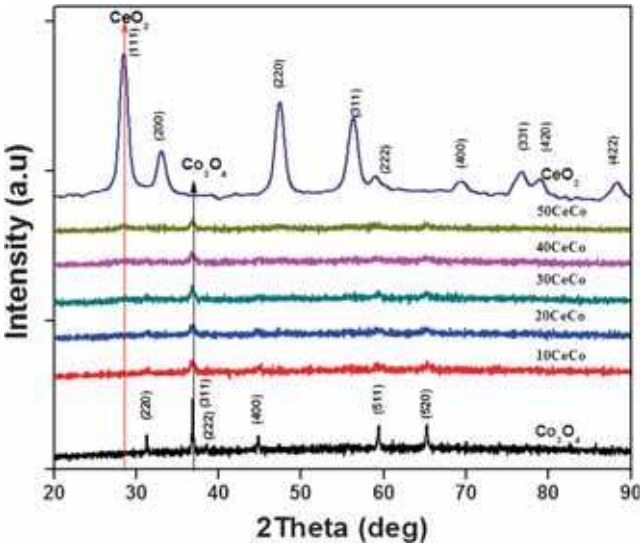

Figure 2. P-XRD patterns of xCeCo catalysts.

Table 1. Surface area, lattice parameters and particle diameter of xCeCo catalysts.

Catalyst	Surface area (m^2g^{-1})	Lattice parameter (Å)		XRD Particle diameter (nm)	
		CeO_2	Co_3O_4	CeO_2	Co_3O_4
Co_3O_4	50	–	8.1801	–	8
10CeCo	65	–	8.1800	15 (10 nm from TEM)	8 (4 nm from TEM)
20CeCo	70	–	8.1800	–	9
30CeCo	72	–	8.1800	–	10
40CeCo	75	–	8.1800	–	12
50CeCo	78	–	8.1800	–	15
CeO_2	80	5.414	–	18	–

Table 2. Surface area of Co_3O_4 catalysts.

Catalyst	Preparatory method	Surface area (m^2g^{-1})
Co_3O_4	Solution combustion	50
Co_3O_4	Co-precipitation	35
Co_3O_4	Hydrothermal	22

Lattice constants of both CeO_2 and Co_3O_4 were calculated and the resulting values are given in Table 1. The CeO_2 lattice constant in pristine ceria catalyst is 5.416 Å. The lattice constant of Co_3O_4 and Co_3O_4 in 90 to 50CeCo is equals 8.18 Å (Table 1).

3.1.2 *Surface area (BET analysis) of Co_3O_4 catalysts*: Specific surface areas of the three Co_3O_4 catalysts are shown in Table 2. As seen in the Table 2, sample prepared by solution combustion synthesis had maximum surface area followed by co-precipitation and hydrothermal synthesis, and the latter had the least specific surface area.

The specific surface area of xCeCo catalysts are given in Table 1. The specific surface area of xCeCo catalyst increased upon CeO_2 loading. Pure Co_3O_4 (solution combustion sample) had specific surface area of 50 m^2g^{-1} but it increased to 78 m^2g^{-1} in 50CeCo catalyst. Pure CeO_2 had the maximum specific surface area (80 m^2g^{-1}). The above results indicate that CeO_2 loading results in formation of small crystallites thereby giving large surface area.[21]

3.1.3 *Raman spectroscopy*

3.1.3a *Co_3O_4catalysts*: Raman spectra of the three Co_3O_4 samples are shown in Figure 3. Co_3O_4 belongs to the space group Oh, Fd_{3m} and bulk Co_3O_4 has five major Raman active modes around 194, 482, 522, 618 and 691 cm^{-1} assigned to F_{2g}, E_g, F_{2g}, F_{2g} and A_{1g}, respectively. The most intense A_{1g} peak (691 cm^{-1}) is assigned to the octahedral site CoO_6 symmetry and the E_g and F_{2g} peaks are together assigned to the tetrahedral site CoO_4 symmetry.[22,23] All the samples give the characteristic peaks, however the intensity of these peaks are different.

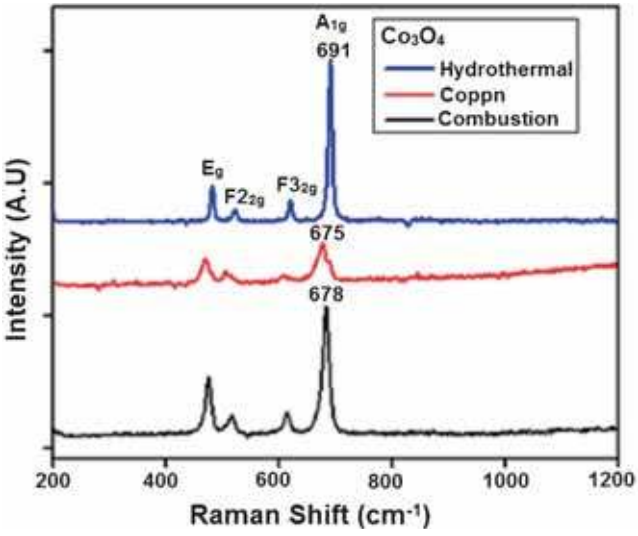

Figure 3. Raman spectra of Co_3O_4 catalysts prepared by different methods.

3.1.3b *xCeCo catalysts:* Raman spectra of xCeCo samples prepared by combustion synthesis are shown in Figure 4. CeO_2 is much more Raman active than Co_3O_4 and shows only one characteristic Raman peak at 464 cm^{-1}.[24] As the content of CeO_2 increases, the 484 cm^{-1} peak of Co_3O_4 gets masked by CeO_2 peak. Also the intensity of both A_{1g} and F_{2g} modes of Co_3O_4 decreases with the increase in CeO_2 content. There occurs a considerable broadening of peaks too. It might be due to change in the composition of Co_3O_4 oxide; change in Co^{+2} : Co^{+3} ratio. When a perfectly octahedral metal oxide undergoes displacement by other metal ions to generate a mixed metal oxide, its Raman spectrum gets broadened due to interactions between different metals.

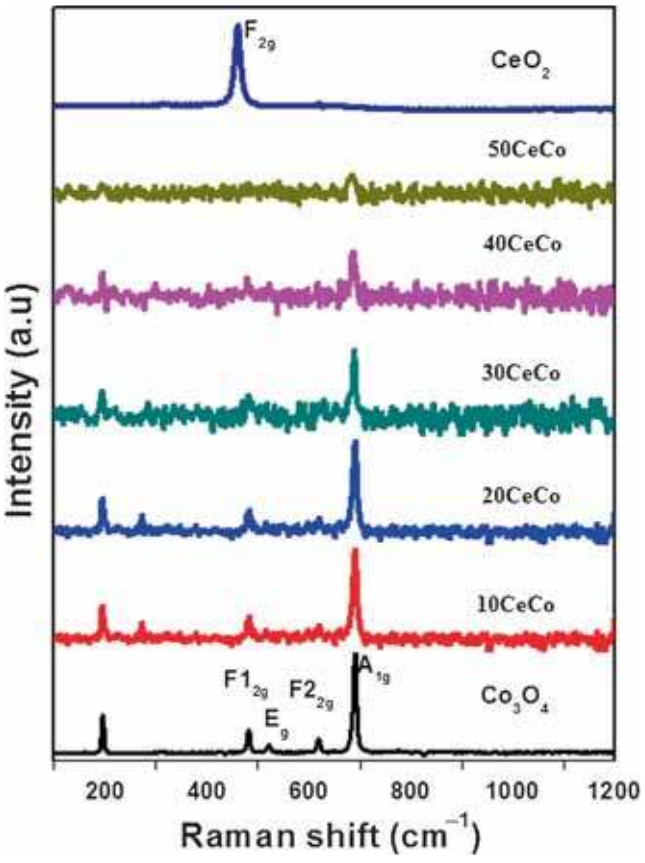

Figure 4. Raman spectra of xCeCo catalysts.

3.1.4 *Diffuse reflectance UV-Vis spectral analyses*

3.1.4a *Co_3O_4 catalysts*: The UV–Visible spectra of the three Co_3O_4 catalysts are shown in Figure 5. There are two bands corresponding to the two transitions occurring in the Co_3O_4 spinel. Both the transitions are ligand to metal charge transfer transitions. The lower wavelength band corresponds to O^{-2} to Co^{+2} transition while the higher energy band corresponds to O^{-2} to Co^{+3} transition.[25]

3.1.4b *xCeCo catalysts*: Figure 6 represents UV-Vis spectra of xCeCo catalysts. The characteristic bands of Co_3O_4 are present in these samples too, however the absorbance changes with the introduction of CeO_2. The lower wavelength band corresponding to O^{-2} to Co^{+2} LMCT transitions suffers a red shift while the higher wavelength band corresponding to O^{-2} to Co^{+3} remains almost unchanged. This implies that CeO_2 doping interacts with Co^{+2} more than Co^{+3} and stabilizes it more. This decreases the energy separation between O^{-2} and Co^{+2} levels which facilitates LMCT transition. This is reflected in the intensities of the two bands. There is an increase in the intensity of first band with an increase in CeO_2 content.

3.1.5 *Temperature programmed reduction (TPR)*

3.1.5a *Co_3O_4 catalysts*: Hydrogen temperature programmed reduction is a very convenient technique for studying the reduction behaviour of catalysts qualitatively. The reducibility of the catalysts plays an important role for supplying of active oxygen. There exists two kinds of oxygen ions on Co_3O_4 surface representing a weaker and stronger local crystal fields sites: one is bonded to one Co^{2+} and one Co^{3+} ion, while the other is bonded to three Co^{3+} ions. The easier surface oxygen abstraction at low temperatures has been connected

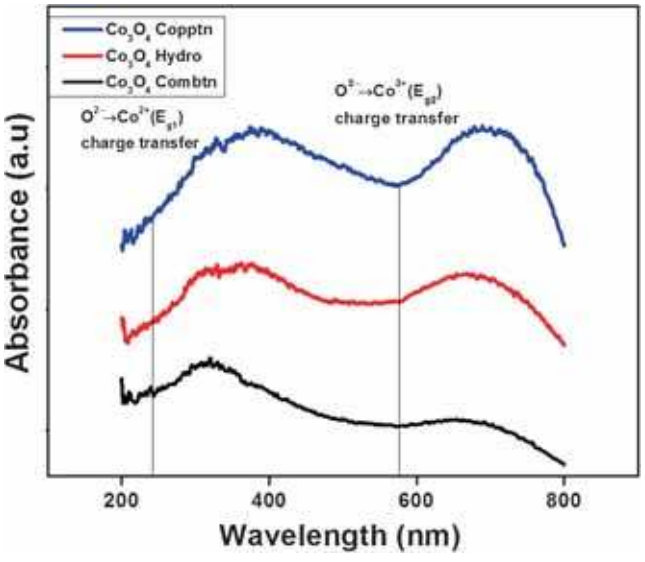

Figure 5. Diffuse reflectance UV-Vis spectra of Co_3O_4 catalysts prepared by different methods.

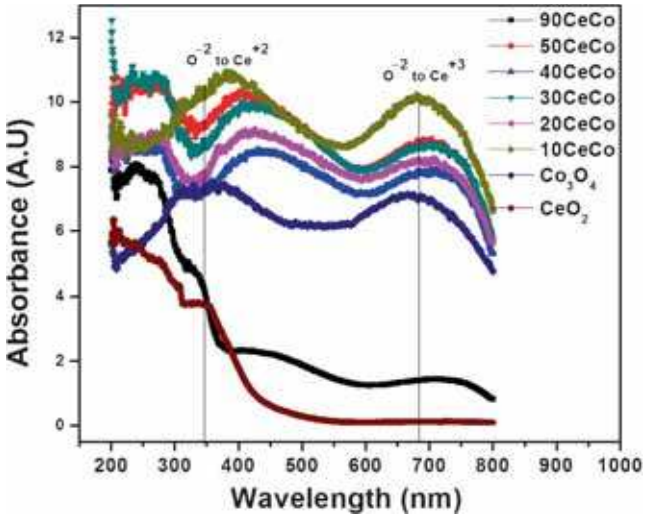

Figure 6. Diffuse reflectance UV-Vis spectra of xCeCo catalysts.

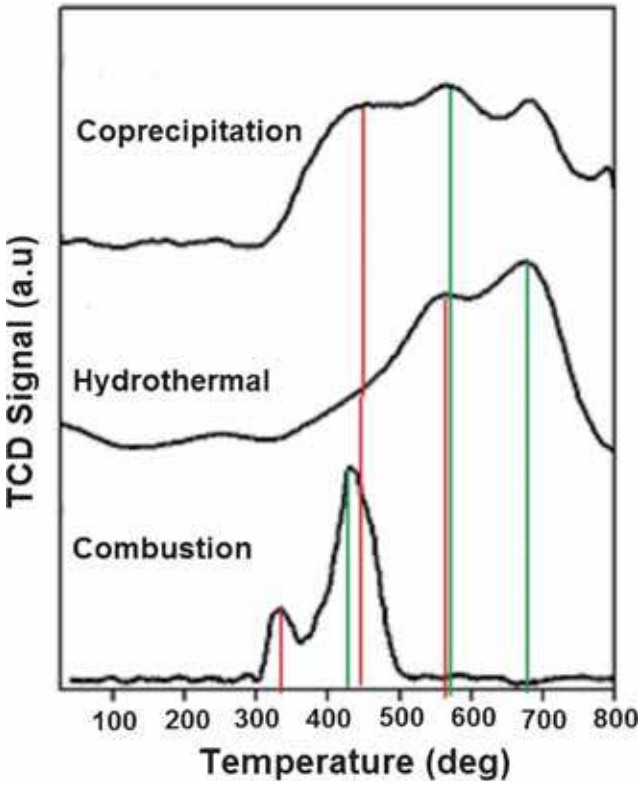

Figure 7. TPR profiles of Co_3O_4 catalysts prepared by different methods.

to the first kind of oxygen bonding. TPR profiles of the three Co_3O_4 catalysts are shown in Figure 7. The lower temperature peak, called the α peak (as shown in red color), corresponds to the reduction of Co^{+3} to Co^{+2} while the one at higher temperature, called β peak (shown in green) is for reduction of Co^{+2} to metallic cobalt, Co.[26] The finding of peak shift in our TPR studies has demonstrated that the reduction behaviour of the samples was influenced by the preparation method. Lowering the reduction profiles of the bulk Co_3O_4 catalyst prepared by combustion method shown in Figure 7 may accompanied by change of shape, crystal structure of Co_3O_4 and the formation of a weaker local crystal field sites of Co^{+2} ions during combustion compared to the bulk Co_3O_4 sample prepared *via* hydrothermal and coprecipitation methods.

3.1.5b *xCeCo catalysts*: Figure 8 shows TPR profiles of xCeCo catalysts. In these catayst too, the two characteristic reduction peaks of Co_3O_4 are present. CeO_2 exhibits 2 reduction peaks in its TPR profile. The first peak is a low temperature peak which appears at about 500°C which is assigned for the reduction of surface capped oxygen. While another high temperature peak at about 800°C corresponds to the reduction of bulk oxygen.[27] Upon introduction of CeO_2, the intensity of

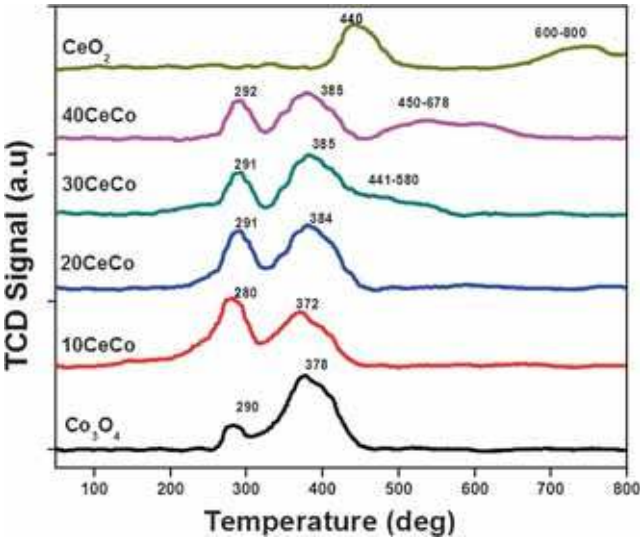

Figure 8. TPR profiles of xCeCo catalysts.

the two Co_3O_4 peaks changes. An increase in CeO_2 content increaes the intensity of α peak and decreases that of β peak. Moreover, a considerable broadening of β peak occurs. The increased intensity implies that more Co^{+3} species are now undergoing reduction as compared to the Co^{+2} species. Also, tailing can be explained by weak reducibility of CeO_2. Thus, presence of CeO_2 makes reduction of Co^{+2} difficult which could be attributed to increased interactions between the two.

3.1.6 *Transmission electron microscopy (TEM)*: Figure 9 shows TEM images taken over the bare CeO_2 support and 10CeCo catalysts. The areas highlighted by the black circles indicate Co_3O_4 particles. Overall, Co_3O_4 particles are well-dispersed throughout the entire CeO_2 particle surfaces examined. The cobalt oxide particles are easily discriminated from the CeO_2 particles, due to their distinct morphological difference. The CeO_2 support has a characteristic rectangular shape as seen in the TEM images of pristine CeO_2, whereas, the Co_3O_4 particles formed after doping of CeO_2 are mostly round. Moreover, the Co_3O_4 and CeO_2 phase identifications have also been confirmed through characteristic lattice structure analysis at high resolution with lattice fringe spacing of 0.24 nm for Co_3O_4 ([3 1 1]) and 0.27 ([1 0 0]) for CeO_2. Lattice parameter values re-establish the fact that the only phases present in the xCeCo catalysts are the individual phases and not mixed oxides.[28]

3.1.7 *X-ray photoelectron spectroscopy (XPS)*: XPS spectra of Co and Ce in 10CeCo are shown in Figure 10. The spectra show Co $2p_{1/2}$ and $2p_{3/2}$ peaks at 795 eV and 780 eV, respectively. Some satellite peaks are also

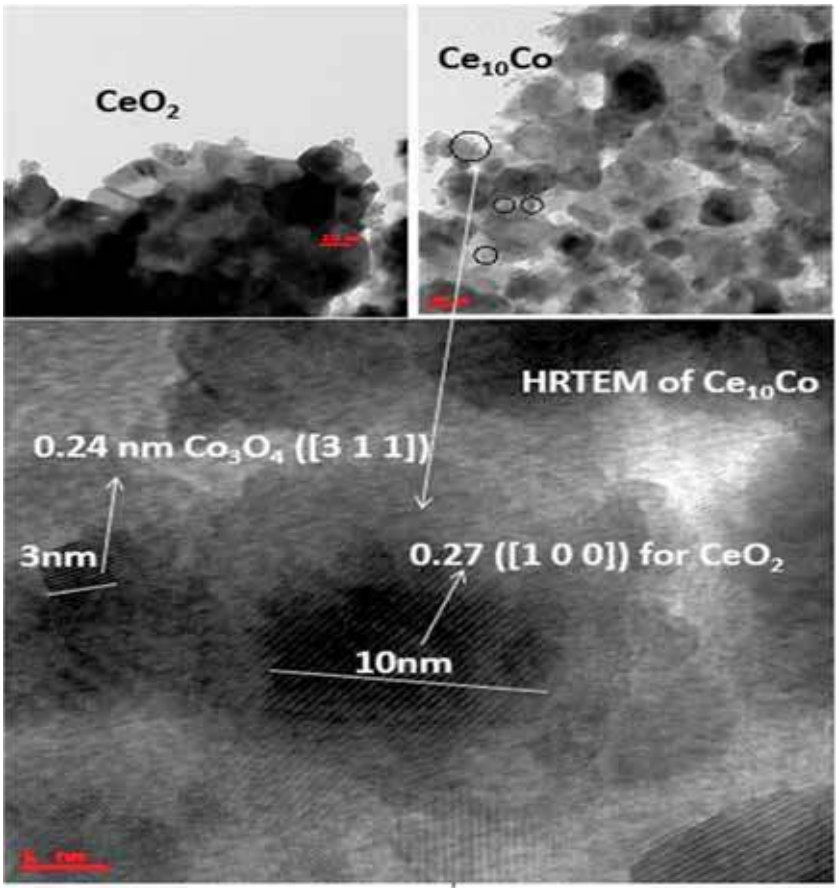

Figure 9. TEM images taken over (a) CeO_2 and (b) 10CeCo; (c) HRTEM of 10CeCo.

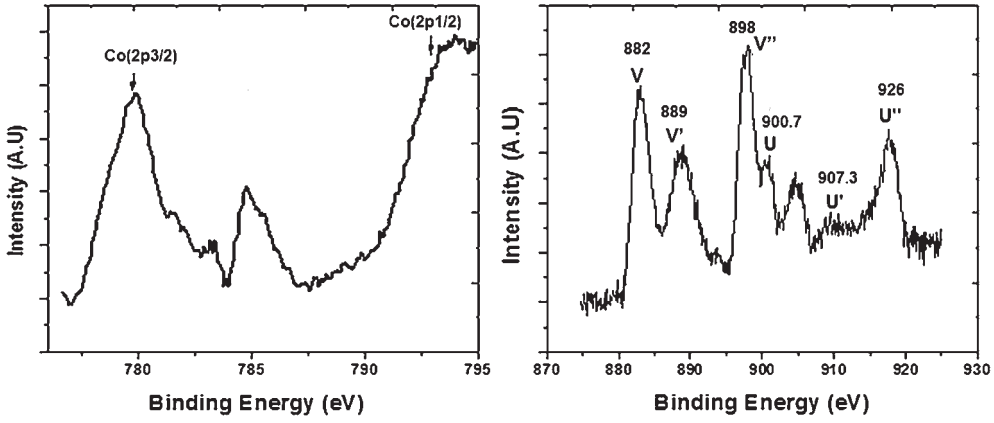

Figure 10. Core level XPS spectra of 10CeCo. (a) Co (2p); (b) Ce(3d).

observed, indicating the presence of both +2 and +3 oxidation states. The XPS spectrum of Ce 3d shows a number of peaks in $3d_{5/2}$ and $3d_{3/2}$ region. These peaks are at 882, 889, 898, 900.7, 907.3 and 916 eV.

3.2 *Catalytic decomposition of N_2O*

3.2.1 *N_2O decomposition by Co_3O_4 catalysts*: Co_3O_4 prepared by three different methods was tested for decomposition of N_2O. The results are shown in Figure 11. Co_3O_4 prepared using combustion synthesis showed best activity among the three catalysts. This could be attributed to the fact that combustion synthesis has the ability to introduce more number of defects in the solid which tend to increase the catalytic activity of the material. Also, it results in nanoparticles having large surface area, which is supported by BET analysis and Raman shift values. According to Raman spectra

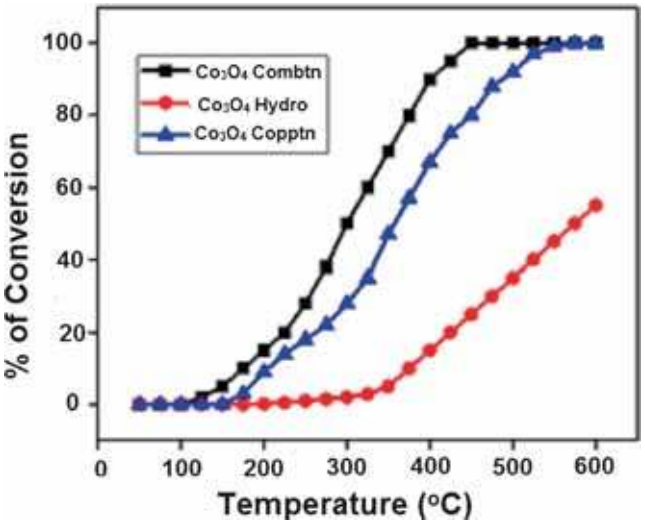

Figure 11. N_2O decomposition by Co_3O_4 prepared by different methods.

(Figure 4), Co_3O_4 sample prepared *via* hydrothermal synthesis has characteristic peaks at nearly the same position as those found in bulk Co_3O_4; however, there occurs a deviation of about 13–16 cm^{-1} in case of coprecipitation and combustion samples.

The reason for the deviation is attributed to the optical phonon confinement in nanostructures, which can cause uncertainty in the phonon wave vectors and thus a downshift in the Raman peaks. This is also supported by the smaller particles formed in case of combustion and coprecipitation synthesis while hydrothermal synthesis generates bulk samples.[29] Since the intensity of a particular peak in Raman spectra is an indication of the number of species responsible for that particular peak, it can be inferred from the above spectra that Co_3O_4 sample prepared from hydrothermal synthesis has more number of octahedral species (Co^{+3}) as compared to the other two samples. Also, the sample prepared *via* combustion synthesis has more number of tetrahedral species (Co^{+2}), as observed in UV-Visible spectra (Figure 5). It is clear from the spectra that there occurs a blue shift in both the bands as one moves from coprecipitation to hydrothermal and combustion samples. This shift could be attributed to the quantum confinement of the nanoparticles which again indicates that combustion synthesis produces nanoparticles. Also, from TPR profiles (Figure 7), it is clear that Co_3O_4 prepared *via* combustion synthesis is an easily reducible species and hence shows better activity than the other two. Hydrothermal sample has these peaks at highest temperature indicating its poor activity. Hence, for furher studies, for preparing CeO_2 supported/doped Co_3O_4 (xCeCo) catalysts, combustion syntehsis was used.

3.2.2 *N_2O decomposition by xCeCo catalysts*: Temperature vs % decomposition graphs of xCeCo catalysts are shown in Figure 12. Introduction of CeO_2 as support to Co_3O_4 improves the activity of the catalyst. However, it is clear from Figure 12 that the promotional effect is strongly dependent on the molar ratio of Ce/Co. In the case of Co_3O_4, the reaction light-off temperature (50% N_2O conversion) is 300°C, and the complete conversion temperature is 450°C. Addition of small amounts of CeO_2 to Co_3O_4 increased the activity, so that 10CeCo catalyst showed maximum activity for this reaction. For 10CeCo catalyst, 50% conversion was achieved at 230°C while 100% conversion was achieved at 350°C. 20CeCo catalyst too had a greater activity than pure Co_3O_4. For this catalyst, the reaction reaches 50% conversion at 250°C and reaches 100% conversion at nearly 380°C.

With further increase of Ce, the promotion effect of CeO_2 on the catalytic activity decreased. Pure CeO_2 was almost inactive for the decomposition of N_2O below 400°C (not shown in Figure 12). From BET surface area it is suggested that the increased surface area is an important factor for the high catalytic activity of 10CeCo. In addition, the presence of appropriate amount of CeO_2 could stabilise the crystallites of Co_3O_4, and thus improve its reduction behaviour. In addition, available active site (Co^{2+}) on the surface of the catalysts decreased because of the surface segregation of CeO_2. Therefore, the catalytic activity of xCeCo ($x > 10$ wt.%) decreased, even though they have larger surface area than 10CeCo. This is because CeO_2 causes better dispersion of Co_3O_4 particles and thus increases the effective surface area available for the reaction. It is clear from the characterization data that CeO_2 interacts with Co^{+2} more than Co^{+3}. Moreover, the activity

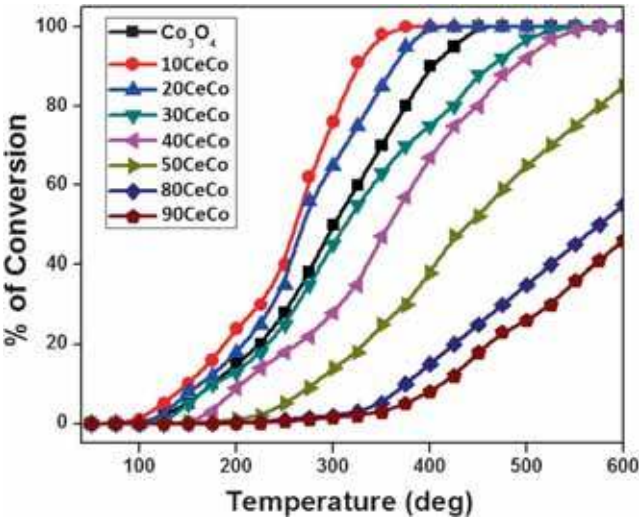

Figure 12. N_2O decomposition by xCeCo catalysts.

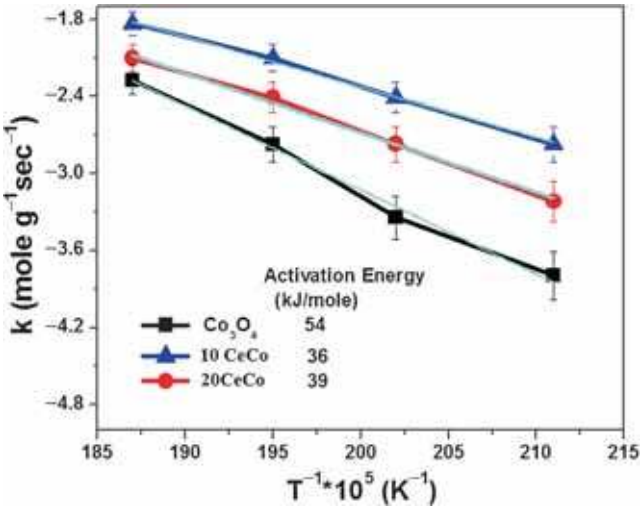

Figure 13. Calculation of activation energy for Co_3O_4, 10CeCo and 20CeCo catalysts.

of catalysts decreases as content of CeO_2 is increased beyond 20 mass%. Hence, it can be proposed that Co^{+2} is the active site for the reaction to occur. More CeO_2 means less availability of Co^{+2} for the reaction. These interactions are favourable at low CeO_2 concentrations, because it leads to a better dispersion and stabilization of the active species. On the other hand, at higher concentrations, CeO_2 might bind more strongly to the active species, thereby rendering them less available for reaction. Activation energies (Ea) of the reaction over xCeCo catalysts are calculated according to the Arrhenius equation and shown in Figure 13.[30–33]

3.2.3 *Activation energy of xCeCo catalysts*: Activation energies (Ea) of the reaction over xCeCo catalysts are calculated according to the Arrhenius equation (Eq-2) and shown in figure 13.[30–33]

$$k = A.e^{-Ea/RT} \quad (2)$$

Around 0.5 g of catalyst was taken and kept inside a quartz tube. N_2O was passed through the inlet at a flow rate of 60 mL min^{-1}. The activation energy varies with the CeO_2 loading and follows the order: Co_3O_4 (54 kJ mol^{-1}) < 20CeCo (39 kJ mol^{-1}) < 10CeCo (36 kJ mol^{-1}). Especially, the value for the 10CeCo sample is lower than the other active catalysts. Comparison of these results with the TEM analysis suggests that the change of surface morphology and the optimal CeO_2 loading can increase both dispersion and surface area of the catalyst and reduces the activation energies that can affect the rate of catalytic N_2O decomposition.

4. Conclusions

In summary, it was shown that preparation methods can affect the activity of the catalyst. Solution combustion method gave the most active Co_3O_4 catalyst for N_2O decomposition and using this we prepared a series of CeO_2 supported Co_3O_4 catalysts to enhance the activity of Co_3O_4. XRD, XPS, FE-SEM and TEM measurements were employed to investigate structural, surface chemical composition as well as the growth process of synthesized nanomaterials and evaluated for N_2O decomposition. With this method, both the size and shape of Co_3O_4 can be controlled under 'one-pot' conditions at relatively low reaction temperatures which can be extended to the preparation of other nanostructures. Lattice oxygen is highly activated because of the Ce introduction and it plays a key role in the decomposition of N_2O and influences the oxygen storage capacity and other properties such as reducibility and reduction temperature. According to the results, it can be concluded that the optimum amount of ceria is 10wt.% (10CeCo). Among these catalysts, the 10CeCo sample exhibits highest surface area and best catalytic activity for N_2O decomposition (T_{50} = 250°C). We propose that an optimal amount of CeO_2 can increase both dispersion and surface area of catalyst and weaken the Co–O bond strength to promote the N_2O decomposition activity.

Acknowledgements

We would like to thank the Council of Scientific and Industrial Research (CSIR), New Delhi, for the award of Senior Research Fellowship. We thank Dr. T.P. Radhakrishnan and DST-Centre for Nanotechnology, University of Hyderabad for TEM analysis.

References

1. Ravishankara A R, Daniel J S and Portmann R W 2009 *Science* **326** 123
2. Caillol S 2011 *J. Photochem. Photobiol. C: Photochem. Rev.* **12** 1
3. Kapteijn F, Rodriguez-Mirasol J and Moulijn J A 1996 *Appl. Catal. B: Environ.* **9** 25
4. Ohnishi C, Iwamoto S and Inoue M 2008 *Chem. Eng. Sci.* **63** 5076
5. Dandekar A and Vannice M A 1999 *Appl. Catal. B: Environ.* **22** 179
6. Haber J, Machej T, Janas J and Nattich M 2004 *Catal. Today* **90** 15
7. Konsolakis M, Aligizou F, Goula G and Yentekakis I V 2013 *Chem. Eng. Sci.* **230** 286
8. Yao K W, Jaenicke S, Lin J Y and Tan K L 1998 *Appl. Catal. B: Environ.* **16** 291

9. Xu X L, Xu X F, Zhang G T and Niu X J 2009 *J. Fuel Chem. Technol.* **37** 595
10. Maniak G, Stelmachowski P, Stanek J J, Kotarba A and Sojka Z 2011 *Catal. Commun.* **15** 127
11. Pieterse J A Z, Booneveld S and Van den Brink R W 2004 *Appl. Catal. B-Environ.* **51** 215
12. Junying W, Haian X, Ju X, Fengtao F, Zhaochi F and Can L 2013 *Chin. J. Catal.* **34** 876
13. Wilczkowska E, Krawczyk K, Petryk J, Sobczak J W and Kaszkur Z 2010 *Appl. Catal. A-Gen.* **389** 165
14. Xie X, Li Y, Liu Z Q, Haruta M and Shen W 2009 *Nature* **458** 746
15. Meng B, Zhao Z, Wang X, Liang J and Qiu 2013 *J. Appl. Catal. B-Environ.* **129** 49
16. Trovarelli A, de Leitenburg C, Boaro M and Dolcetti G 1999 *Catal. Today* **50** 353
17. Campbell C T and Peden C H 2005 *Science* **309** 713
18. Xue L, Zhang C, He H and Teraoka Y 2007 *Appl. Catal. B-Environ.* **75** 167
19. Asano K, Ohnishi C, Iwamoto S, Shioya Y and Inoue M 2008 *Appl. Catal. B-Environ.* **78** 242
20. Liu R S, Iwamoto M and Lunsford J H 1982 *J. Chem. Soc., Chem. Commun.* **1** 78
21. Reddy P S S, Pasha N, Rao M C, Lingaiah N, Suryanarayana I and Prasad P S 2007 *Catal. Comm.* **8** 1406
22. Na C W, Woo H S, Kim H J, Jeong U, Chung J H and Lee J H 2012 *CrystEngComm* **14** 3737
23. Gwag J S and Sohn Y K 2012 *Bull. Korean Chem. Soc.* **33** 505
24. Song H and Ozkan U S 2010 *Catal. A: Chem.* **318** 21
25. Barakat N A, Khil M S, Sheikh F A and Kim H Y 2008 *J. Phys. Chem. C* **112** 12225
26. Li J B, Jiang Z Q, Qian K and Huang W X 2012 *Chin. J. Chem. Phys.* **25** 103
27. Boaro M, Vicario M, de Leitenburg C, Dolcetti G and Trovarelli A 2003 *Catal. Today* **77** 407
28. Xu X L, Xu X F, Zhang G T and Niu X J 2009 *J. Fuel Chem. Technol.* **37** 95
29. Farhadi S, Pourzare K and Sadeghinejad S 2013 *J. Nanostructure Chem.* **3** 1
30. Mahammadunnisa S, Reddy P M K, Karuppiah J and Subrahmanyam Ch 2013 *Adv. Chem.* **1** 264
31. Baidya T, Dutta G, Hegde M S and Waghmare U V 2009 *Dalton Trans* **3** 455
32. Megarajan S K, Rayalu S, Teraoka Y and Labhsetwar N 2014 *J. Mol. Catal. A: Chem.* **385** 112
33. Tang C W, Kuo M C, Lin C J, Wang C B and Chien S H 2008 *Catal. Today* **131** 520